POAC'17
Busan, KOREA

Proceedings of the 24th International Conference on
Port and Ocean Engineering under Arctic Conditions
June 11-16, 2017, Busan, Korea

New Insights about Ice Friction Obtained from Crushing-Friction Tests on Smooth and High-Roughness Surfaces

Robert E. Gagnon[1]
[1] Ocean, Coastal and River Engineering, National Research Council Canada,St. John's, NL, Canada

ABSTRACT

Ice crushing-friction tests were conducted in the lab at -10 ºC using a set of acrylic ice-crushing platens that included a flat smooth surface and a variety of high-roughness surfaces with regular arrays of small prominences. The experiments were part of Phase II tests of the Blade Runners technology for reducing ice-induced vibration. Ice was crushed against the platens where the ice movement had both a vertical and a horizontal component. High-speed imaging through the platens was used to observe the ice contact zone as it evolved during the tests. Vertical crushing rates were in the range 10 – 30 mm/s and the horizontal sliding rates were in the range 4.14 – 30 mm/s. Three types of freshwater ice were used. Friction coefficients were extraordinarily low and were proportional to the ratio of the tangential sliding rate and the normal crushing rate. For the rough surfaces all of the friction coefficient variation was determined by the fluid dynamics of a slurry that flowed through channels that developed between leeward-facing facets of the prominences and the moving ice. The slurry originated from a highly-lubricating self-generating squeeze film of ice particles and melt located between the encroaching intact ice and the surfaces. These results are important because ice crushing occurs in many situations that involve a sliding frictional component such as sports involving ice-contact, ice interaction with bridges, piers, ship hulls, rock beds under glaciers and ice-on-ice sliding/crushing within glaciers and extraterrestrial ice masses (on Saturn's moon Enceladus) and between interacting sea ice floes.

KEY WORDS: Ice crushing-friction; Highly-lubricating ice-melt slurry; Solid-solid fluid interface friction mechanism; Surprising low friction on rough surfaces.

INTRODUCTION

As pointed out by Gagnon (2016), the frictional behavior of ice has been studied in many contexts, such as in relation to cold-environment sports involving friction on sled runners, skate blades and curling rocks, in the automotive industry concerning rubber tire performance on ice, in shipping regarding friction on hulls of icebreaking ships and other vessels in cold regions, in construction regarding the friction of moving ice on concrete such as piers, bridges and other fixed river and marine structures, in the movement of glaciers regarding ice-on-rock and ice-on-ice friction, and even in relation to extraterrestrial ice-on-ice friction in tectonically active regions of the icy Saturnian moon Enceladus. Over the past few decades ice crushing and indentation have also been studied intensively, mostly in relation to ice engineering associated with offshore oil and gas resources. The main characteristics of the ice behavior consistently recur during field and lab studies and at various scales (Gagnon, 1999). While ice

friction in nature often involves some degree of crushing, as in most of the cases above, only a few studies have been conducted specifically on the topic of ice crushing friction where substantial crushing is an integral component (Gagnon and Mølgaard, 1989). Here we present results from ice crushing-friction tests, using novel apparatus, on high-roughness surfaces that reveal new friction mechanisms where the friction coefficient depends on both the normal crushing rate and the tangential sliding rate, and is extraordinarily low.

PRELIMINARY CONSIDERATIONS

To set the stage for discussing ice crushing friction we first consider an ice feature crushing against a surface where no lateral sliding of the ice feature is involved. Many studies (Gagnon, 1999; Riska et al., 1990; Fransson et al., 1991) have shown that during the crushing there are regions of relatively intact ice, small compared to the nominal contact area, in the contact zone that are surrounded by crushed ice which flows away from the intact zones (Fig. 1a). The peripheral crushed ice is essentially the debris of shattered spalls that have previously broken away sequentially from the intact hard zone. Fig. 1a shows a spall-creating fracture (dashed line) that is about to occur. When the spall forms (to the left of the fracture) and separates from the intact bulk ice it immediately shatters and pulverizes to become crushed ice. Thin section analysis from lab tests confirmed the intact nature of the ice (Gagnon, 1994) and thin and thick sections from the Hobson's Choice Ice Island indentation tests (Gagnon, 1998) showed similar features. The pressure on the intact ice zones (hard spots) is very high (30-70 MPa) and changes abruptly to low values (0-10 MPa) when crossing the boundary between intact ice and the crushed material at the perimeter. The high-pressure zones have been shown to be regions where a thin squeeze-film slurry layer of pressurized melt and ice particles is present between the intact ice and the surface (Fig. 1). The viscous flow of this slurry layer generates heat that accounts for the rapid melting component of the removal of ice from the hard zones during ice crushing. A similar process occurs at ice-on-ice contact (Gagnon, 2013) of ice fragments in the surrounding crushed ice matrix as it flows away from the high-pressure zones.

SLURRY LAYER DETAILS

Details of the thin layer have been the subject of investigation in four previous studies. Gagnon (2016) has summarized the results and provided a general view of the nature of the slurry layer during crushing for tests at a similar scale to that of the present ones. We can surmise that the slurry layer thickness in the present tests is somewhere in the approximate range 0.02 mm - 0.17 mm, and the liquid fraction of the layer is about 16%. We may think of the slurry layer as a self-generating squeeze film that is powered by the energy supplied by the loading system that causes the ice crushing.

EXPERIMENTAL SETUP

Fig. 2a shows a photograph of the test setup where the ice, confined in a rigid holder, is pressed in the vertical direction at a fixed rate against a transparent acrylic crushing platen (2.5 cm thickness) in a testing frame. Note that in Fig. 1 the ice is situated above the platen, for illustrative purposes, whereas in the actual tests (Fig. 2a) the ice was positioned below the platen. The crushing platen is backed by a secondary polished acrylic support plate (5 cm in thickness). The ice holder is attached to the top face of a 2.5 cm thick metal plate. The plate has four commercial 'frictionless' ball-bearing cars attached under it that ride on two metallic

rails in the horizontal direction parallel to the long axes of the ice specimen and the crushing platen. An electric actuator is used to move the plate and ice holder at controllable fixed rates.

High-speed images of the ice-platen contact region are recorded by viewing through both the support plate and the crushing platen by means of a mirror situated between the supporting posts for the plate and platen. Each of the two platens primarily discussed here had either an array of small regular square pyramids machined onto its surface (Fig. 2b) or an array of

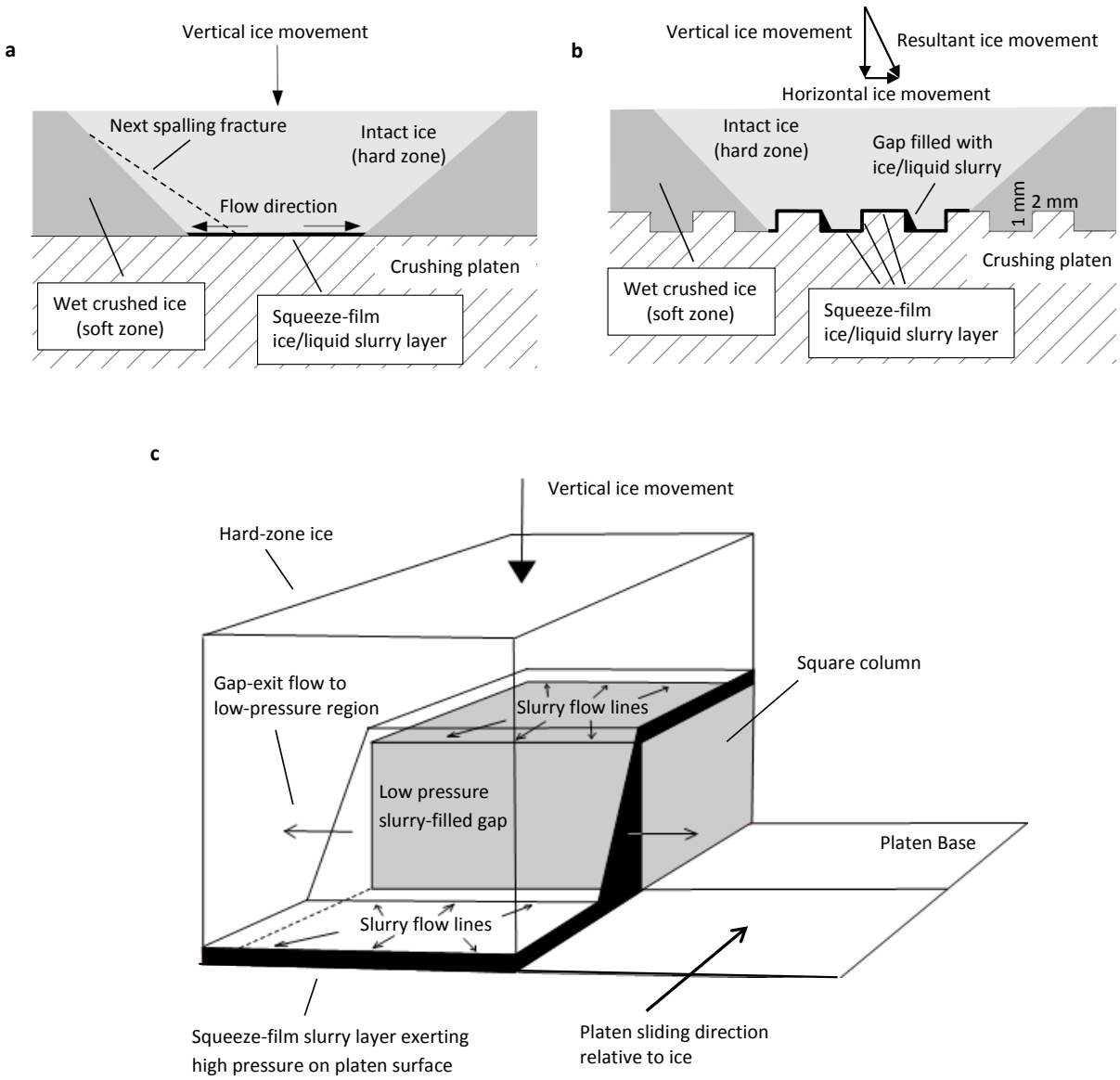

Fig. 1. Schematics showing aspects of the ice behavior during the crushing-friction experiments. **(a)** Schematic showing the essential characteristics of ice crushing against a flat rigid surface. **(b)** A 2D schematic depicting ice crushing against a platen surface with square columns. The ice has both a vertical and a horizontal component of movement relative to the crushing platen, where the resultant movement is as indicated. **(c)** A 3D schematic showing a small portion, a unit area containing one square column, of the view of the ice and platen shown in Fig. 1b. The schematic depicts the time-averaged general flow characteristics of the self-generating squeeze-film slurry as it moves from high-pressure regions, where it is generated, into the lower-pressure gap space and eventually out through the gap exits where low-pressure crushed ice is present. From Gagnon (2016).

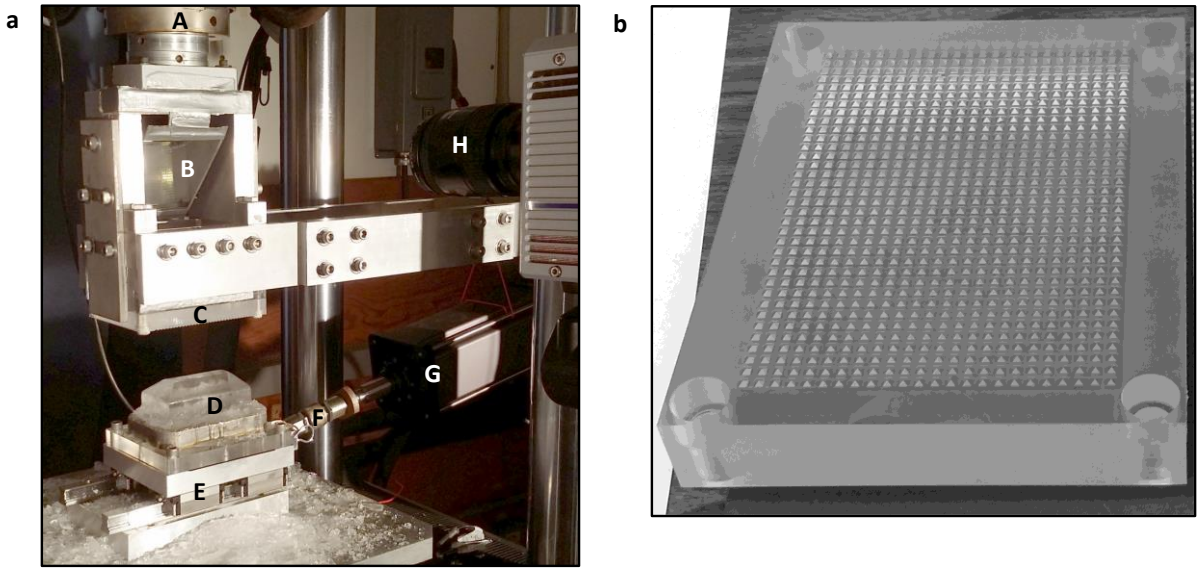

Fig. 2. Test apparatus photographs. **(a)** Photograph of the crushing-friction test setup. (A) Vertically-oriented test-frame load cell for measuring the normal load; (B) Mirror; (C) Acrylic crushing-platen; (D) Ice specimen in ice holder; (E) Rail-car assembly; (F) Load cell used to measure the horizontal friction force; (G) Linear actuator used to slide the rail-car and ice sample horizontally; (H) High-speed imaging camera. **(b)** Photograph of the acrylic platen with the array of small regular square pyramids on its surface (platen dimensions: 166 mm x 129 mm x 25 mm). The pyramids were 1 mm in height and 2 mm wide at the base. The space between each adjacent pyramid was 2 mm. The arithmetic average of the high-roughness profile for the surface of the platen was 0.075 mm. From Gagnon (2016).

square columns with the same base dimensions, height and spacing as the pyramids. The pyramids were 1 mm in height and 2 mm wide at the base. The space between each adjacent pyramid was 2 mm. The arithmetic average of the high-roughness profiles for the surfaces of the two platens were 0.075 mm (square pyramids) and 0.375 mm (square columns).

Most of the ice samples were prepared from freshwater granular ice blocks grown in the lab (grain size ~ 4 mm). Some ice samples were prepared from a columnar-grained freshwater ice sheet grown in a basin (column diameter ~ 5 mm). During tests the columnar grains were orthogonal to the vertical crushing direction and the long axis of the ice sample. Each ice sample was approximately 7 cm in height, and 12 cm by 6.5 cm at its base. The top of the samples was given a rounded-wedge shape. Each sample's base was freeze-bonded to an ice holder consisting of an acrylic plate with a rectangular band of steel (2 cm in height) attached to it that encompassed the base of the ice specimen. The ~ 1 cm gap between the ice sample and the confining steel band was filled with snow and then saturated with water near 0 ^{o}C so that, when frozen, it provided confinement at the base of the ice sample to prevent it from shattering during testing. Tests were carried out at –10 ^{o}C and the load data from the vertical crushing actuator and the horizontal sliding actuator were acquired at 6144 samples per second. The vertical crushing rates used for these tests were 10, 20 and 30 mm/s. The horizontal sliding rates used were 4.14, 10, 12.42 and 20 and 30 mm/s. All ice samples were crushed to a depth of ~ 35 mm.

TEST RESULTS AND DISCUSSION

Friction Data Characteristics

Fig. 3 (Top and Bottom) show the friction coefficient results for the tests conducted using the crushing platen with the array of pyramids. The reasonably good consistency of repeated test results is evident. Noteworthy observations from Fig. 3 (Top) are: (1) The friction coefficients are extraordinarily low given the high degree of roughness of the crushing platen. For comparison Fig. 3 (Top) includes two data points corresponding to two low-roughness unprepared flat steel plates, where each point represents the average friction coefficient value of two tests. (2) The friction coefficient increases with the horizontal sliding speed for any given vertical crushing rate. For the data corresponding to the 10 mm/s vertical crushing rate the friction coefficient dependence on sliding speed is roughly fitted by a line. (3) The friction coefficient is constant for the tests (Box A, excluding steel plate data) conducted at a constant ratio of vertical crushing rate and sliding speed, i.e. where the vertical crushing rate and the horizontal sliding rate ratios are (10 mm/s : 10 mm/s), (20 mm/s : 20 mm/s), and (30 mm/s : 30 mm/s). Below these data points on the chart are three other pairs (Box B) that demonstrate essentially the same thing, although the second pair of data points does not have exactly the same ratio as the first and last pair, (10 mm/s : 4.14 mm/s), (20 mm/s : 10 mm/s), and (30 mm/s : 12.42 mm/s). (4) The slopes of the three fit lines on the chart for the pyramids platen diminish as the vertical crushing rate increases. All of these observations may be understood in the context of the explanation of the ice behavior given below.

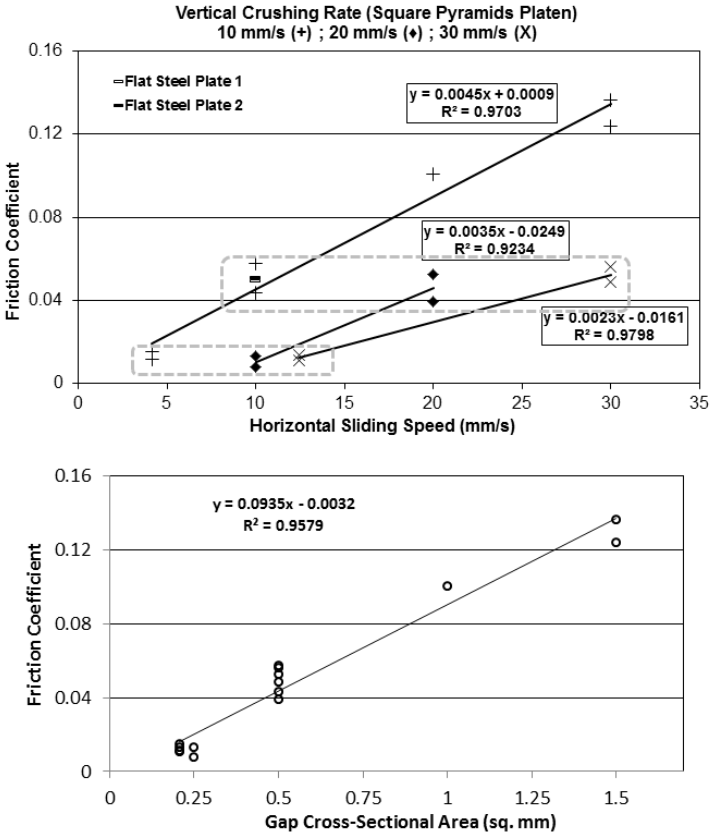

Fig. 3. Main friction coefficient results for the tests using the crushing platen with the array of square pyramids. (Top) Friction coefficient versus horizontal sliding speed. Tests corresponding to three vertical crushing rates and five horizontal sliding rates were conducted.

The included data points corresponding to the tests conducted using the two flat steel plates represent averages of two tests in each case, where the vertical crushing rate and horizontal sliding speed were both set at 10 mm/s. Scatter in the data, that is inherent in ice crushing and friction experiments, amounted to about ± 15%. (Bottom) Friction coefficient versus gap cross-sectional area. Granular ice was used for all tests shown in this figure. From Gagnon (2016).

Most of the experiments were conducted using the platen with the array of pyramids. Some tests were performed using the platen with the array of square columns (Fig. 4), including a few using columnar-grained freshwater ice that yielded very similar results. The friction values and slope of the fitted line are greater than that for the platen with the pyramid array (Fig. 3, Top). This is due to the higher roughness value for the platen with the square columns (0.375 mm) as opposed to 0.075 mm for the pyramids platen. Fig. 5 shows data from all platens used for friction tests. Table 1 describes these platens. The generally low friction coefficients and increase in values with sliding speed seen in Figs. 3 and 4 is evident for all platens with rough surfaces tested at two sliding speeds shown in Fig. 5.

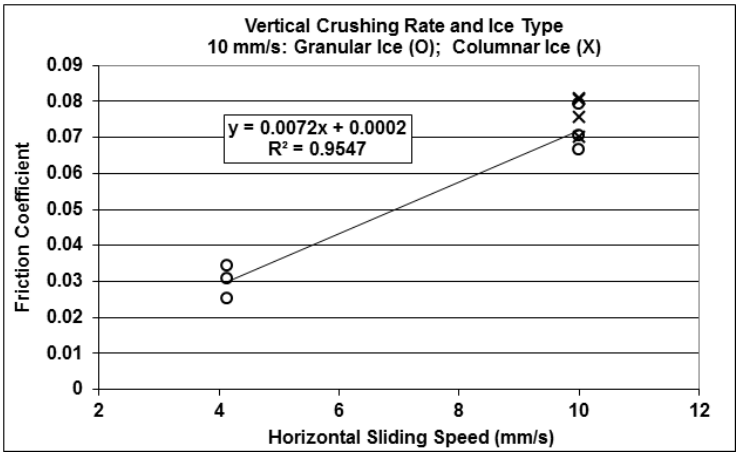

Fig. 4. Friction coefficient versus horizontal sliding speed for tests using the crushing platen with the array of square columns. Scatter in the data, which is inherent in ice crushing and friction experiments, amounted to about ± 15%. Granular ice was used for six tests and columnar ice was used for four tests. From Gagnon (2016).

Regarding ice crushing friction on high-roughness non-ice surfaces, the only data available are those presented in this paper. Similarly, the only analytical formulation to explain the data is found here, so comparisons with other studies are not possible as yet. On the other hand, the mechanisms described here, i.e. the inherent presence of the lubricating slurry and its fluid dynamic characteristics with respect to roughness features, are new and they may have some relevance to ice friction in cases where a degree of ice crushing (at some scale) occurs, such as on asperities under curling rocks, when skate blades plough/gouge the underlying ice and when rough edges of sea ice floes slide/grind against one another.

High-Speed Imaging Data of the Ice-Platen Interface

Fig. 6 shows an image from the high-speed image record of a test using the crushing platen with the array of square columns. The view is through the transparent acrylic crushing platen and the grid of small square columns is apparent. We see a roughly centrally-located horizontally-elongated dark hard zone that consists of relatively intact ice where the pressure is high (~ 53 MPa (Gagnon 2016)). The relatively intact hard zone appears dark because a thin sheet of black plastic was placed between the actuator head and the ice holder so that the black sheet was visible through the translucent ice sample and ice holder in areas where there was no opaque crushed ice (the white material). The elongated shape of the hard zone is due to the shape of the original ice sample (a horizontal wedge) that provides confinement governed by its geometry (Spencer and Masterson, 1993). The hard zone is surrounded by white material that consists of low-pressure (0-10 MPa) pulverized spall debris that is flowing away from the high-pressure region, generally extruding along the channels between the columns.

Table 1. Platen #, material, blade and array description/dimensions.

Platen #	Material	Blade and Array Description (all 'blades' are 1 mm in height)
2	Acrylic	Symmetric Crossed-Bars (45^o wedged-shaped bars, 2 mm wide x 8.6 mm long); normal staggered array; 8.5 mm center-to-center spacing for rows and columns
5	Aluminum	Horizontal 45^o Wedge Bar (8.6 mm long and 2 mm wide); normal staggered array; 8.5 mm center-to-center spacing for rows and columns; sliding perpendicular to bars
7	Acrylic	Horizontal 45^o Wedge Bar (8.6 mm long and 2 mm wide); dense staggered array; 4.25 mm center-to-center spacing for rows and 8. 5 mm for columns; sliding along bars
11	Acrylic	Square Column (2 mm x 2 mm); square array; 4 mm center-to-center spacing
12	Acrylic	Square Pyramid (2 mm x 2 mm); square array; 4 mm center-to-center spacing
13	Acrylic	Square Column (2 mm x 2 mm); square array; 4 mm center-to-center spacing
14	Acrylic	Square Pyramid (2 mm x 2 mm); square array; 4 mm center-to-center spacing
16	Steel	Unprepared flat steel plate
20	Steel	Unprepared flat steel plate

FRICTION MECHANISMS AND FURTHER ANALYSIS

Schematics of the Physical Processes

In Fig. 6 the ice sample is sliding horizontally (to the right in the image) at the same rate (10 mm/s) as it is crushing vertically against the platen. The same processes described above for the ice crushing against the platen in the vertical direction apply to the ice crushing horizontally against the vertical walls of square columns facing the encroaching ice. For the intact hard zone to move horizontally to the right the thin squeeze-film slurry layer must be effectively removing hard-zone ice that is contacting the vertical walls of the square columns.

Fig. 1b shows a 2D schematic depicting ice crushing against a surface with square columns. Fig. 1c shows a 3D view of a smaller portion of that shown in Fig. 1b, containing only one square column. Although most of the data presented here is for the case of the platen with the square pyramids, we focus on the platen with square columns in the illustrations and associated discussion because the geometry and discussion are easier to depict and follow. The principles at play that are inculcated in the discussion, however, are the same in both cases. As discussed above the ice/surface contact consists of relatively-intact centrally-located hard-zone ice that is surrounded by crushed ice, i.e. shattered spall debris, at the sides of the

hard zone. Between the hard zone and the underlying surface, either at the flat base of the platen or a vertical wall of a square column encroached by ice, is the heat-generating thin squeeze-film slurry layer that melts and erodes hard-zone ice as it flows. The slurry wets the crushed ice in its vicinity wherever it exits the high-pressure zone. The squeeze-film slurry dissipates the majority of the actuator energy supplied to the system because the load is mostly borne on the hard-zone ice (~ 88%, Gagnon (1994)), where the slurry is generated and flows. Consequently the energy dissipation rate of the slurry is directly proportional to the rate of crushing on whatever surface the ice crushes against, i.e. at horizontal surfaces or vertical surfaces of the platen.

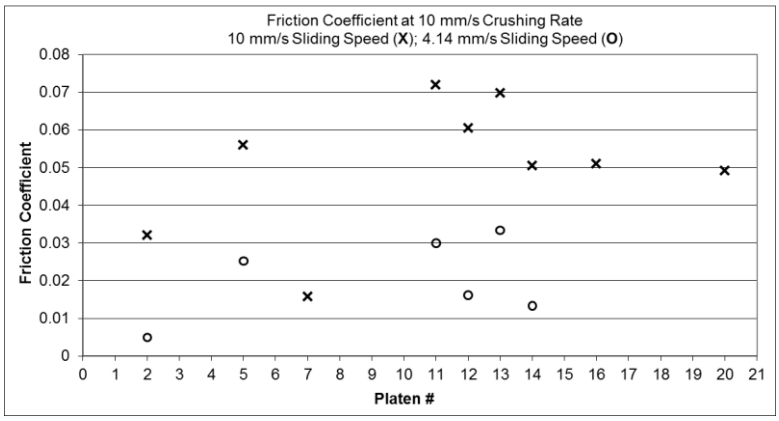

Fig. 5. Friction coefficient data for several of the platens used in the test program. Data points represent averages of multiple tests.

In Fig. 1b the ice crushes against the platen in the downward direction at a fixed rate and the ice is sliding horizontally to the right at a fixed rate. Since the actual movement of the ice relative to the platen is in the direction shown and since the ice is being melted and eroded on the tops of the square columns the shape of the ice in the space between two adjacent square columns will have a gap at the trailing left side, in the shape of a right wedge. The top angle of the right wedge is equal to the arctangent of the horizontal sliding speed divided by the vertical crushing rate. Hence the cross-sectional area of the gap is proportional to the horizontal sliding speed divided by the vertical crushing rate. The gap will be filled with flowing slurry since pressurized slurry will enter from the top of the square column and from the base of the platen in front of the gap, where the contacting hard-zone ice is melting/eroding, and will exit the gap at its sides where the pressure is lower, that is, in and out of the view of the figure. More detail on this is given below. In Fig. 1b the difference in pressure on the square column walls that face the oncoming ice and the lower pressure on the column walls on the leeward side of the oncoming ice, where the slurry-filled gaps are, accounts for the friction force. To give a better perspective of the gap, Fig. 1c shows a 3D view of a smaller portion of that shown in Fig. 1b, containing only one square column. This represents a unit area on the platen surface. Fig. 1c is a simplified schematic of what in reality is a highly dynamic situation. Gagnon (2016) noted that during a crushing-friction test a typical hard zone grows in size for certain time intervals and also suddenly, and frequently, diminishes in size by small amounts whenever small spalls break away from it at various locations. Furthermore, the hard zone is quite mobile (from the imaging records) in the vertical sense of Fig. 6 while remaining centrally located on average. In reality, due to these factors, the patterns and directions of flow of the pressurized slurry layer varies considerably both spatially and temporally, hence Fig. 1c represents a simplified time average of events.

The slurry fluid flows out of the sides of the gap where pressure is low because there is frequently low-pressure crushed ice in the immediate vicinity of one or both sides of the gap. This is due to the narrow width (a few times the width of a square column, or less) and elongated shape of the high-pressure zones, as seen in Fig. 6.

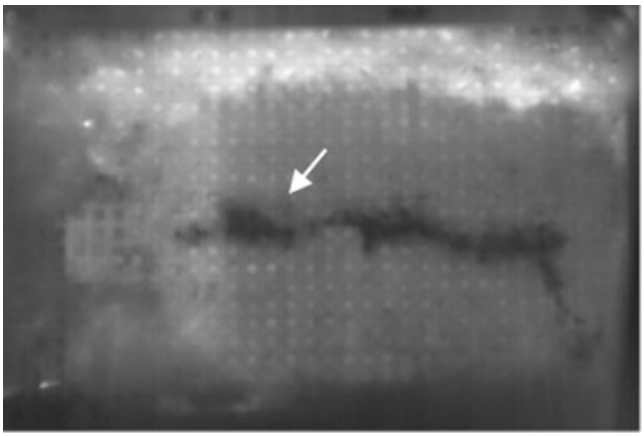

Fig. 6. An image from the high-speed image record of a test using the crushing platen with the array of square columns where the vertical crushing rate and horizontal sliding speed to the right were both set at 10 mm/s. The view is through the transparent acrylic crushing platen. A horizontally-elongated dark hard zone that consists of relatively intact ice, where the interface pressure is high, is visible. The hard zone is surrounded by crushed ice (the white material). The arrow points to a small region where a spalling event had occurred shortly before the image was captured. The width of the image is ~133 mm.

Analytical Description of the Friction Force

To analytically describe the friction force we need to know the parameters that determine the average pressure that the slurry exerts on the vertical column face in the gap. In the time-averaged sense, the gap acts somewhat as a short length of pipe or channel through which slurry flows. However, the geometry in Fig. 1c is clearly more complex than that of a simple channel and we would not expect that standard theory for flow within a channel would apply. Indeed in the present case all we know is that fluid enters the gap (channel) from the top of the column and base of the platen and exits at the sides of the gap. A complicating factor is that the pressurized slurry is entering the gap (channel) along its whole length, a very different scenario from fluid entering one end of a channel and exiting at the other end. For the average pressure of the gap slurry in the present scenario we might expect some sort of dependence on gap cross-sectional area. Due to the complexities of the geometry and flow entry characteristics, however, the analytical derivation of such a dependence from first principles is beyond the scope of this work.

Fortunately, all of the friction data in Fig. 4 (Top) for the platen with the square pyramids turns out to be proportional to the cross-sectional area (A) of the gap (Fig. 4, Bottom), where for geometrical simplicity we have assumed that the platen had square columns, i.e. where $A \approx \frac{1}{2}$ (horizontal sliding speed)/(vertical crushing rate) mm^2. While different in magnitude the cross-sectional areas of the gaps for the square pyramids would nevertheless be proportional to cross-sectional areas of gaps for square columns, as attested by the good fit in Fig. 4 (Bottom). To reiterate, the same proportional dependence of friction coefficient on gap cross-sectional area applies to both square pyramids and square columns. The above points

imply that in these tests the average pressure that the slurry exerts on the column face within the gap is proportional to a constant maximal area minus the cross-sectional area of the gap. The friction coefficient is written as:

$$\mu = n\, w\, (P - P_{gap})/L = n\, w\, (P - P\, (A_{max} - A)/ A_{max})/L \quad (1)$$

where μ is the coefficient of friction, n is the number of square columns in the hard-zone area, w is the area of a column face, P (~ 55 MPa) is the slurry (squeeze-film) pressure on a column face on which ice is encroaching, P_{gap} is the average pressure of the flowing slurry on a column face in the gap, L is the normal crushing load, A_{max} is a certain constant area, and A is the cross-sectional area of the gap where $A_{max} > A$. The form of P_{gap} in equation (1), $P\, (A_{max} - A)/ A_{max}$, derives from Fig. 3 (Bottom) that stipulates that the friction coefficient is proportional to A and tends to zero as A tends to zero, while P_{gap} tends to P as A tends to zero. Since we know that the gap cross-sectional area has the form stated above, equation (1) further simplifies and reduces to:

$$\mu = n\, w\, P\, A / (A_{max}\, L) = n\, w\, P\, H^2\, V_h / (2\, V_c\, A_{max}\, L) \quad (2)$$

where H is the height of a column, V_h is the horizontal sliding speed and V_c is the vertical crushing rate.

The ice crushing-friction coefficient of a flat polished acrylic or aluminum surface is extremely low, virtually not resolvable with our apparatus, as indicated in the few tests that were conducted on flat acrylic and aluminum platens. Therefore equations (1) and (2) do not include any contribution to the friction force from ice crushing against the machined (near-polished) flat base of the platens in the areas between the square columns or square pyramids.

Equations (1) and (2) are essentially stating that the friction coefficient is directly proportional to the gap cross-sectional area A, as is evident in Fig. 4 (Bottom). Gagnon (2016) previously noted that the contribution to the friction force from the crushed ice (visible in Fig. 6) is negligible compared to that of the hard-zone ice. While equation (2) specifically relates to a platen with square columns, the patterns and trends of the data presented in Fig. 4 (Top) for the square-pyramids platen are nevertheless reflected in the equation. Gagnon (2016) investigated typical values for the two unknown quantities in equation (2), n and A_{max}, and obtained the following mutually reasonable estimates, n ~18 and A_{max} ~1.5 mm^2.

CONCLUSIONS

The generation and flow characteristics of a thin ice/liquid slurry layer, with respect to the regular array of prominences on the platen surfaces, explains the low magnitudes and the trends in the friction data. This viscous layer removes hard-zone ice from the contact interface through melting and erosion (Gagnon, 2016). The layer may be thought of as a self-generating squeeze film that is powered by the energy supplied by the loading system that causes the ice crushing. On flat relatively smooth surfaces the squeeze-film slurry layer causes extremely low friction forces. These friction mechanisms have not been observed before.

These results have beneficial consequences for the potential use of scaled-up panels with arrays of protrusions (Gagnon, 2015) that could be used to reduce ice-induced vibration of structures (e.g. offshore wind turbines and oil platforms) without causing undesirable high friction forces. Conversely, rough surfaces designed to have a high friction coefficient (e.g.

anti-slip surfaces on wheels or tracks) may have unexpectedly low friction coefficients when ice is crushed against them. The flow of glaciers may be influenced by the friction mechanisms described here at the glacier bases where ice slides over uneven rock surfaces. It was noted that the flowing slurry layer served to clean corrosion from the surfaces of unprepared steel plates. There may be specialized cleaning applications of natural or prepared hard surfaces, with low or high degrees of roughness, where ice crushing and sliding across the surface would be effective and non-contaminating, involving only short-duration exposure to tiny amounts of liquid water with no other cleaning agents.

The presence of a thin squeeze-film layer of ice/liquid slurry produced by ice crushing on flat aluminum and acrylic surfaces in this study specifically led to extremely low friction coefficients. This should be considered when attempting to explain the frictional behavior of skate blades, sled runners and curling stones where local crushing on ice asperities and/or small-scale ice unevenness, and due to gouging/plowing, occurs. By the term 'ice crushing' we include the production of the thin squeeze-film slurry layer both during spalling events and in the time intervals between spalling events.

ACKNOWLEDGEMENTS

The author would like to thank OCRE/NRC for its support of this research. The author is also grateful to Austin Bugden for technical assistance during the test program.

REFERENCES

Fransson, L., Olofsson, T., Sandkvist, J. 1991. Observations of the failure process in ice blocks crushed by a flat indentor. Proceedings of the 11th International Conference on Port and Ocean Engineering Under Arctic Conditions, 1, 501 514.

Gagnon, R.E., 1994. Generation of melt during crushing experiments on freshwater ice. Cold Regions Science and Technology, 22(4), 385-398.

Gagnon, R.E., 1998. Analysis of visual data from medium scale indentation experiments at Hobson's Choice Ice Island. Cold Regions Science and Technology, 28, 45-58.

Gagnon, R.E., 1999. Consistent observations of ice crushing in laboratory tests and field experiments covering three orders of magnitude in scale. *Proceedings of POAC-99*, **2**, 858-869.

Gagnon, R.E. and Mølgaard, J., 1989. Crushing friction experiments on freshwater ice. *Proceedings of the IUTAM/IAHR Symposium on Ice/Structure Interaction*, 405-421.

Gagnon, R.E., 2013. High-speed imaging of ice-on-ice crushing. *Proceedings of POAC 2013*, Paper No. 159.

Gagnon, R.E., 2015. Large scale spallation inducing ice protection. US Patent 9,181,670 B2, Nov. 10.

Gagnon, R.E., 2016. New friction mechanisms revealed by ice crushing-friction tests on high-roughness surfaces. Cold Regions Science and Technology, 131, 1-9.

Riska, K., Rantala, H., Joensuu, A., 1990. Full scale observations of ship ice contact. Laboratory of Naval Architecture and Marine Engineering, Helsinki University of Technology, Report M 97.

Spencer, P.A. and Masterson, D.M., 1993. A geometrical model for pressure aspect-ratio effects in ice-structure interaction. Proceedings of OMAE 1993, 4, 113-117.